SASEC2015
Third Southern African Solar Energy Conference
11 – 13 May 2015
Kruger National Park, South Africa

COMPUTATIONAL FLUID DYNAMICS ANALYSIS OF PARABOLIC DISH TUBULAR CAVITY RECEIVER

Craig, K.J.*, Le Roux, W.G. and Meyer J.P.
*Author for correspondence
Department of Mechanical and Aeronautical Engineering,
University of Pretoria, Pretoria, 0002, South Africa,
E-mail: ken.craig@up.ac.za

ABSTRACT

The paper describes the Computational Fluid Dynamics (CFD) analysis of a parabolic dish tubular cavity receiver. The analysis uses the geometry of an experimental setup and considers experimental conditions as well as ideal conditions linked to a Brayton cycle microturbine implementation. The CFD analysis comprises of two parts. First, the Radiative Transfer Equation (RTE) is solved with a Finite Volume (FV) method using the Discrete Ordinates (DO) method for the optical performance of the dish and receiver to obtain the absorbed radiation on the receiver tube. In this method both an axi-symmetric model with a ring-like receiver is considered utilizing a 2-D mesh as well as a 3-D model with the spiraling tubular receiver. The former is much less computationally intensive because of the extra dimension but simplifies the receiver shape. The result of this FV simulation is an absorbed radiation distribution that is patched as volumetric heat source in the second CFD simulation. This simulation is a conjugate heat transfer model that evaluates the heat transfer to the heat transfer fluid as well as the losses from the cavity insulation and due to thermal re-radiation. The method is evaluated for an ambient lower pressure experimental test at the University of Pretoria as well as a theoretical implementation at Brayton cycle conditions.

INTRODUCTION

Parabolic dish Concentrated Solar Power (CSP) plants have the benefit of providing a thermal energy solution for remote areas. This CSP application differs from other plants (Parabolic trough, Linear Fresnel, solar tower) in that the receiver with heat transfer fluid is located at a central point that has to move with the reflector to track the sun. This means that typical heat engines for this type of plant include the Stirling engine and potentially a Brayton cycle device, as evaluated in the current study. The state of the art of Stirling dishes are summarized by Siva Reddy et al [1] and Mancini et al [2]. Le Roux et al [3,4] have investigated the feasibility of a Brayton cycle application and performed optimization studies using ray tracing and thermodynamic relations and network heat transfer models. Certain assumptions regarding the thermal boundary conditions and solar load were made in those studies. This paper performs an alternative analysis using Computational Fluid Dynamics (CFD) in attempt to provide more detailed information as to temperature distributions, absorbed radiation profiles and to validate or confirm the experimental results obtained [4], thereby providing a platform for subsequent optimization studies. The receiver type used in the current work is a tubular receiver that is simpler to implement experimentally than a volumetric receiver [5]. The CFD analysis in this paper will lay the groundwork for optimization of the receiver layout.

NOMENCLATURE

a	[-]	Absorption coefficient
I	[W/sr]	Radiative intensity
n	[-]	Refractive index
l	[m]	Mixing length
N	[-]	Number
T	[K]	Local temperature
q	[W/m^2]	Radiative flux in non-gray medium

Special characters

β	[-]	Extinction coefficient
λ	[m]	Wavelength
τ_w	[N/m^2]	Wall shear
σ_s	[-]	Scattering coefficient
ϕ	[-]	Phase function
Ω'	[sr]	Solid angle
$\nabla.$	[-]	Divergence operator
$\vec{s}'$	[-]	Scattering direction vector
$\vec{r}$	[-]	Position vector
$\vec{s}$	[-]	Direction vector

Subscripts

θ	Angular direction	b	Black body
ϕ	Angular direction	N	Number of ordinate directions
λ	spectral	z	Cartesian axis direction

DESCRIPTION OF GEOMETRY

The geometry considered in this study corresponds to the experimental setup of Le Roux et al, [3,4] and is shown in Figure 1. The critical dimensions of the facility are listed in Table 1.

Figure 1 Experimental setup of parabolic dish and tubular receiver [4]

Table 1 Dimensions of dish and receiver [4]

Dish radius [m]	2.4	Dish focal length [m]	2.897
Aperture dimensions [m]	0.25x0.25	Rim angle [°]	45
Tube outer diameter [mm]	88.9, schedule 10		

The computational domain for the CFD model is shown in Figure 2 with a plot of the mesh on the tubular receiver in Figure 3. The dish is modelled as a smooth parabolic reflector without the struts evident in the experimental setup (Figure 1). The support struts that hold the receiver are neglected as far as their influence on the radiation concentrated onto the receiver is concerned. Faceted insulation is placed in front of the receiver aperture, partially shading the lower surface of the tubular pipe. Solar irradiation enters through the top surface with specified Direct Normal Irradiation (DNI) and a subtended beam angle of 0.53° and reflects off the paraboloid reflector with a specified reflectivity.

CALCULATION OF SOLAR LOAD ON RECEIVER

The determination of the non-uniform solar heat flux distribution around the absorber tubes of a tubular cavity requires the solution of the Radiative Transfer Equation (RTE).

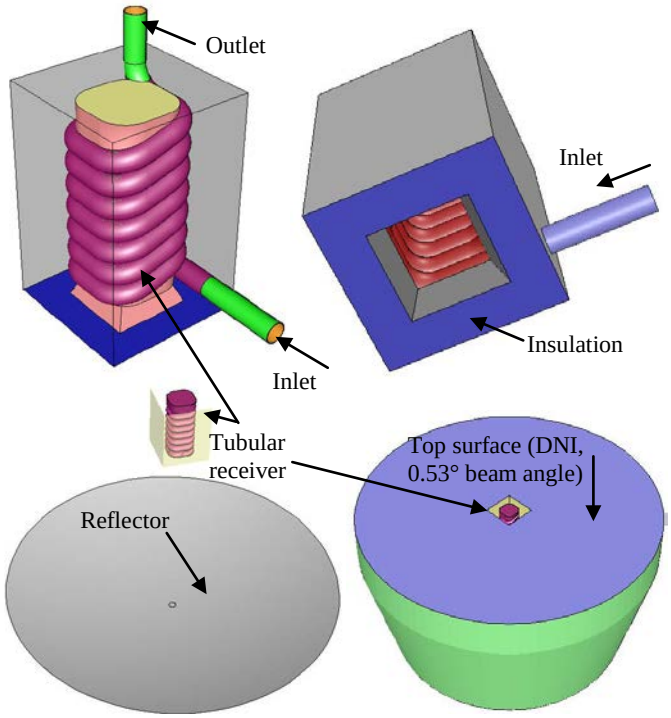

Figure 2 Computational domain of parabolic dish and receiver

Table 2 Material characteristics of dish reflector and receiver [4]

Item	Material	Optical quantity	Value
Reflector	Mill-finished Aluminium	Reflectivity	0.55
Receiver tube	Stainless steel 316	Solar Absorptance, α_s	0.85
		Total hemispherical emissivity	0.7

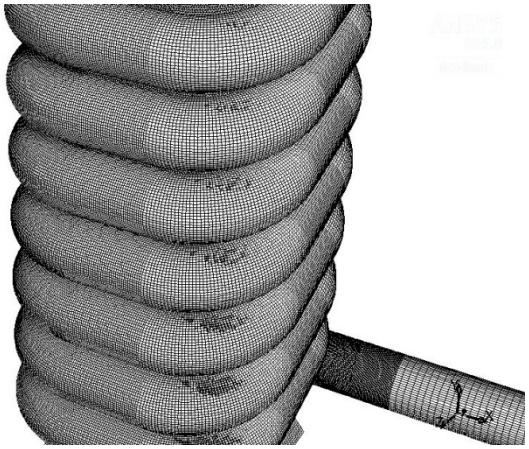

Figure 3 Computational mesh on tubular receiver

The RTE describes the balance of energy through the interaction of emission, absorption and scattering in a participating medium. Imagine a beam with a radiative intensity of $I_\lambda(\vec{r},\vec{s})$ which is a function of the spectral wavelength variable (λ), position ($\vec{r}$) and direction ($\vec{s}$) that

travels in an absorbing, scattering, and emitting medium in the aforementioned direction. On the one hand, the beam energy decreases due to absorption and its scattering from its initial trajectory to other directions (out-scattering), while on the other hand, its energy increases due to medium volume thermal radiation emission and scattering from other trajectories towards its trajectory (in-scattering). Mathematically, this is expressed as [6]:

$$\nabla.\left(I_\lambda(\vec{r}.\vec{s})\,\vec{s}\right)+\beta_\lambda I_\lambda(\vec{r}.\vec{s})=a_\lambda n^2 I_{b\lambda}+\frac{\sigma_{s\lambda}}{4\pi}\int_0^{4\pi} I_\lambda(\vec{r}.\vec{s}')\phi(\vec{s}.\vec{s}')d\Omega' \qquad (1)$$

where $\beta_\lambda = a_\lambda + \sigma_{s,\lambda}$ and the summation of all terms on the right hand side is called the source term. Moreover, the radiative flux definition for a non-gray medium is

$$q(r)=\int_0^{\infty}\int_0^{4\pi} I_\lambda(\vec{r}.\vec{s})\,\vec{s}\,d\Omega' d\lambda \qquad (2)$$

By double integration of the RTE equation over all solid angles over all wavelengths, the divergence of heat flux can be calculated as

$$\nabla \bullet q=\int_0^{\infty} a_\lambda\left(4\pi I_{b\lambda}-\int_0^{4\pi} I_\lambda(\vec{s}')d\Omega'\right)d\lambda \qquad (3)$$

The divergence of the radiative heat flux is determined in ANSYS Fluent [7] with the S_2 method, a subset of the Discrete Ordinates (DO) using the S_N approach, where N is number of ordinate directions. The angular space is subdivided into $N_\theta \times N_\phi$ control angles, each of which is further subdivided by pixels in the two angular directions. For 1-D, $2\times N_\theta \times N_\phi$ directions of the RTE equations are solved, for 2-D, $4\times N_\theta \times N_\phi$ directions, while for 3-D, $8\times N_\theta \times N_\phi$ directions are computed, implying that the computational overhead and memory requirements increase linearly with each angular discretization division and that for each spatial dimension that is added, the overhead doubles.

The FV implementation of the RTE equation leads to both false scattering (or numerical diffusion) and a ray effect [8]. The first causes smearing of the propagated radiation while the second causes an incorrect direction of the wave front. In ANSYS Fluent, these can be reduced by three methods: refining the mesh, increasing the number of angular discretizations, and increasing the order of the spatial discretization of the DO method.

The solution of the DO equation is challenging for a 3-D geometry like the parabolic dish under consideration. In order to determine mesh-independent solutions, a 2-D axi-symmetric geometry is first considered and then compared to a much more expensive 3-D FV of the RTE equation.

The total absorbed radiation on the pipe of the tubular receiver is plotted against the $N_\theta \times N_\phi$ value in Figure 4 for both the axi-symmetric and 3-D models using the material properties in Table 2. The reflectivity of the dish is low due to the mill-finish used on the aluminium. The following observations can be made:

- A change from first- to second-order discretization of the DO equation results in an increased total absorbed radiation
- Changing the DNI from 1 000W/m^2 to 747W/m^2 and the dish reflectivity from 100% to 55% is confirmed in the CFD simulation to purely obey the arithmetic ratio of 0.747*0.55
- It can be seen that a value of $N_\theta \times N_\phi$ of 80x80 gives a result that is approaching asymptotic convergence in terms of total absorbed radiation.
- It can also be seen that the 3-D result is similar to the axi-symmetric result in terms of total absorbed radiation for the same $N_\theta \times N_\phi$ values (see insert), and that a scaling factor may be applicable to transform a lower 3-D $N_\theta \times N_\phi$ distribution to a distribution adhering to the correct total absorbed radiation.

Both the DO 80x80 axi-symmetric model (utilizing a 2-D mesh of about 17000 cells with $4\times N_\theta \times N_\phi$ DO equations) and the DO 25x25 coarsest mesh 3-D model (with 1.7M cells and $8\times N_\theta \times N_\phi$ equations) require a large amount of memory to solve (90GB and 120GB, respectively).

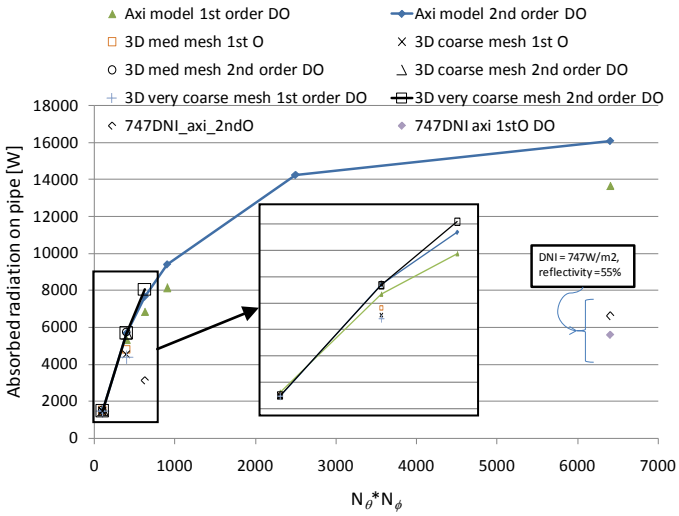

Figure 4 Total absorbed radiation [W] on receiver tube for axi-symmetric and full 3D model as a function of DO $N_\theta \times N_\phi$ (insert showing close-up for low values of DO $N_\theta \times N_\phi$), mesh density and DNI (all DNI values 1 000W/m^2 except those indicated)

The incident radiation contours is displayed for both axi-symmetric and 3-D cases in Figure 5. It can be seen that there is a marked difference in the focusing between the axi-symmetric and 3D results, with the 3-D results being more spread out in the vicinity of the receiver. As mentioned above, the full 3-D became prohibitively expensive for higher $N_\theta \times N_\phi$ values, so the comparison has to be limited to 25x25 (Figure 5a versus 5c). The peak values of incident radiation are larger for the axi-symmetric model than for the 3-D mode due to the reflective nature of the axis boundary condition.

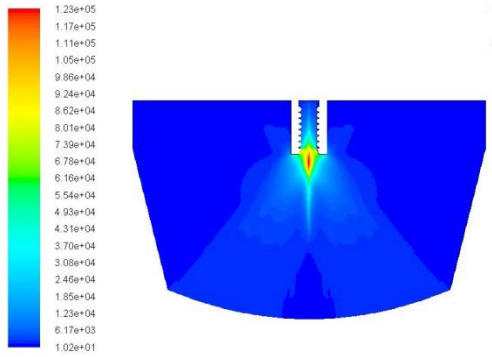

a) Axi-symmetric model: DO 25x25,Tube α_s=0.85

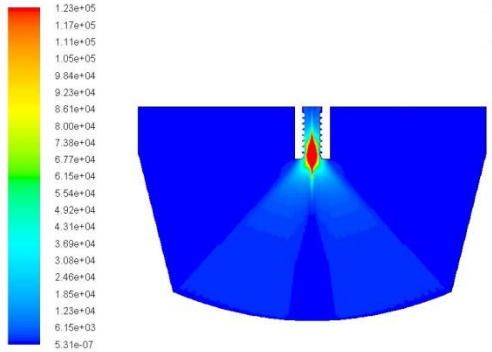

b) Axi-symmetric model:DO 80x80, clipped at 123kW/m^2, Tube α_s=1

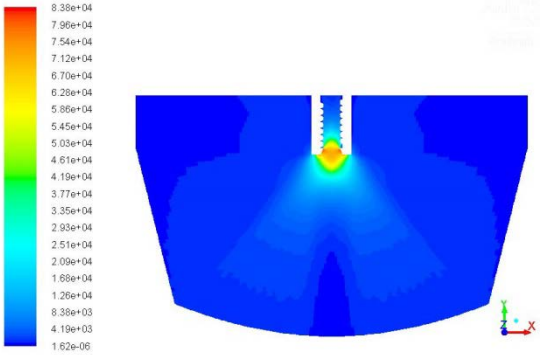

c) 3-D model: DO 25x25, Tube α_s=1
Z=0 surface

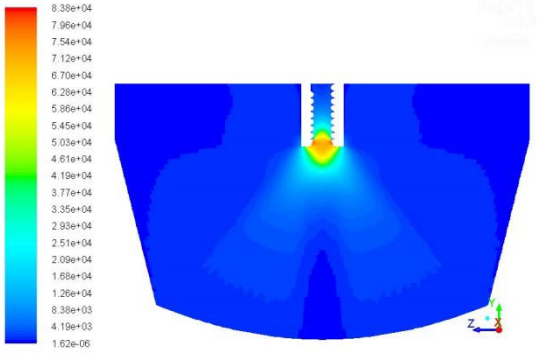

d) 3-D model: DO 25x25, Tube α_s=1
X=0 surface

Figure 5 Incident radiation contours [W/m^2] for axi-symmetric and full 3D model (DNI=747W/m^2, 55% reflectivity)

The absorbed radiation levels for the axi-symmetric and 3-D models are however similar (Figure 6), although with a different distribution along the receiver height. The shadowing effect of the receiver can be seen on the incident radiation contours on the reflector surface in Figure 7.

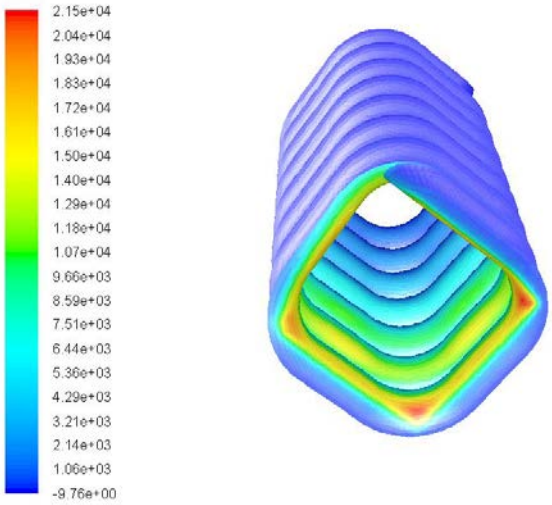

a)

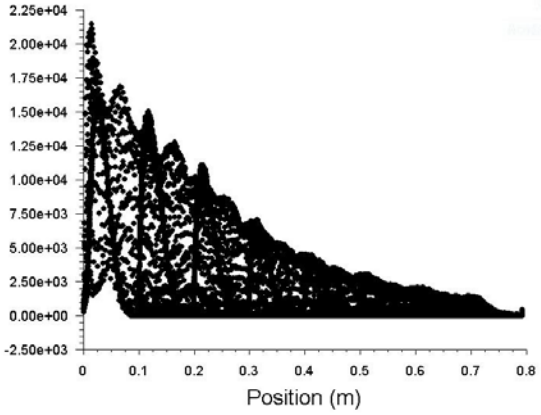

b)

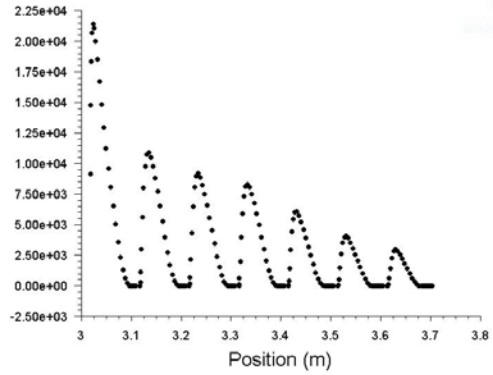

c)

Figure 6 Absorbed flux [W/m^2] on receiver tube FV RTE (DNI=747W/m^2, 55% reflectivity, DO 25x25,Tube α_s=1) a) contours of absorbed radiation flux on tube (3-D model), b) Versus receiver height (3-D model), c) Versus receiver position (axi-symmetric model)

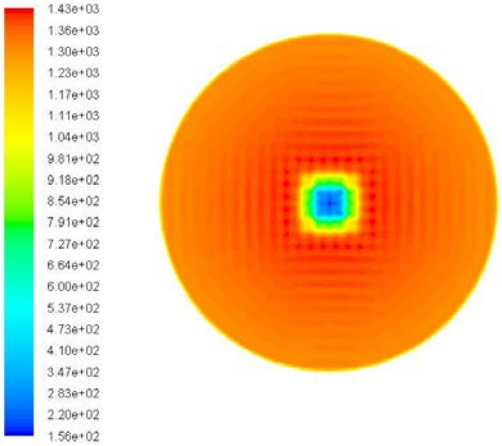

Figure 7 Incident radiation contours [W/m^2] on reflector (DNI=747W/m^2, 55% reflectivity, DO 25x25,Tube α_s=1)

PROCESSING OF SOLAR LOAD

Once the solar load has been determined with the FV solution of the RTE equation, it is applied as a volumetric heat source in a 3-D conjugate heat transfer CFD model of the receiver, using the following procedure [9]:

1. Convert absorbed radiation (solar load) on collectors into interpolation file, scaling the data by dividing by the thickness of the receiver tube. This converts the flux [W/m^2] to a volumetric heat source [W/m^3].
2. Define a User-defined scalar (UDS).
3. Interpolate data to UDS.
4. Copy UDS to User-Defined Memory (UDM) using a User-Defined Function (UDF).
5. Assign source term using UDF to patch load as volumetric heat source.

The result of the procedure is shown in Figure 8 in the form of UDM contours on the tube surface and a plot of the UDM on the pipe versus receiver height. The 3-D model data were scaled by a factor of 2.492 to have the same integrated value as the 80x80 DO axi-symmetric case.

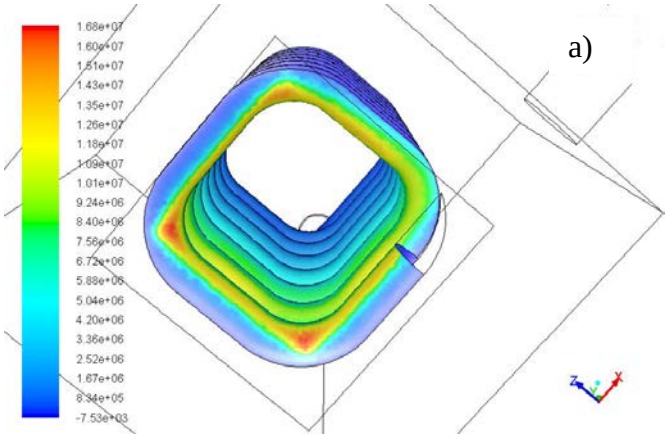

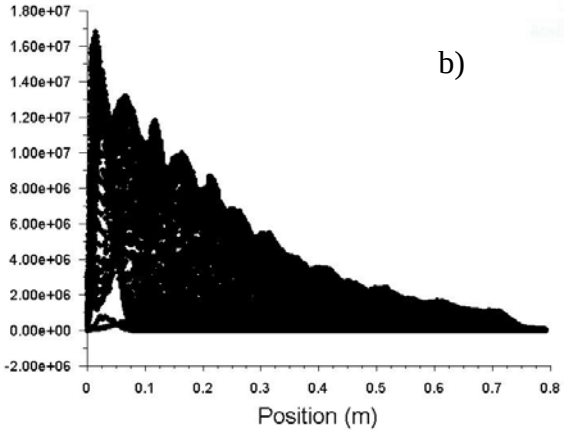

Figure 8 Volumetric heat source of absorbed radiation [W/m^3] on receiver tube FV RTE (DNI=747W/m^2, 55% reflectivity, DO 25x25, Tube α_s=1) scaled to DO 80x80 axi-symmetric model value: a) contours, b) Versus receiver height

CONJUGATE HEAT TRANSFER CFD MODEL RESULTS

Case 1 - Ambient test condition

Table 3 lists the boundary conditions used for the 3-D conjugate heat transfer model. The first test case corresponds to Test A, Day 2, Blower setting 3 in Ref. 2.

Table 3 Boundary conditions for 3-D CFD thermal simulation (Cases 1 and 2)

Surface	BC type	Boundary value
Inlet HTF (Case 1)	Mass-flow inlet	0.0983 kg/s; 292K
Inlet HTF (Case 2)	Mass-flow inlet	0.08 kg/s; 1070K
Outlet	Pressure outlet	0Pa gauge
Tube outer surface facing cavity	Opaque wall	0.85 emissivity
Cavity aperture	Semi-transparent wall	-
Insulation sides and top	Mixed thermal condition	292K (T_{conv}); h_c=5 W/m^2-K 271 (T_{rad} =T_{sky})
Insulation bottom	Mixed thermal condition	292K (T_{conv}); h_c=5 W/m^2-K 296K (T_{rad})

Sample CFD results are given as insulation temperatures (Figure 9), outlet temperature profile indicating swirl due to the spiral of the tube (Figure 10) and static pressure contours (Figure 11) confirming the pressure drop across the receiver.

Table 4 summarizes the results. The temperature rise in the HTF obtained is higher than that measured (Case 1a). The main reason for this is the slope error of the experimental dish that was not incorporated into the CFD model. According to Ref.2, there was a significant amount of spillage of radiative flux around the receiver aperture that would reduce the amount of absorbed radiation. The spillage was estimated using a SolTrace model of the receiver of the experimental setup combined with a thermal model [8]. When adjusting the applied computational solar load to match the total experimentally estimated tube power, the results labelled as Case 1b in Table 4 are obtained. The outlet temperature is now slightly under-predicted but much closer to the experimentally measured value.

Case 2 - Brayton cycle condition

For this case, an ideal condition from Ref.3 was picked with the inlet values listed in Table 3. The input DNI was adjusted to 1000W/m^2 and the inlet temperature increased to a typical Brayton cycle value. No tracking error is assumed because of the perfect nature of the CFD model geometry during the ray tracing. The resulting outlet temperature obtained is listed in Table 4. In Ref.3, the incoming solar irradiation captured by the dish is listed as 18.1kW. The integrated heat source applied in the current model only amounted to 14.2kW. Ref.3 also specifies an optical efficiency, whereas this efficiency is implicitly taken into account in the two CFD models. Further investigation is required to correlate the deviation.

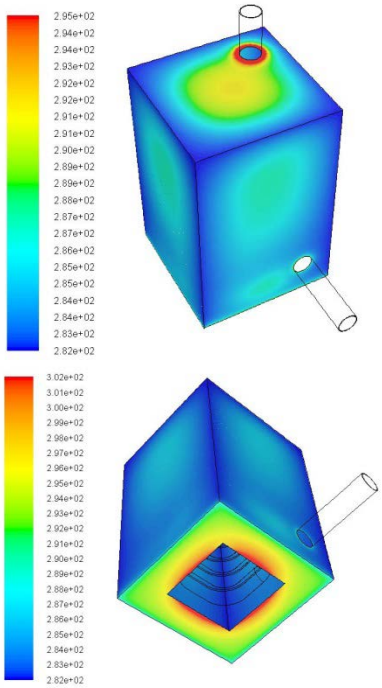

Figure 9 Temperature contours [K] on insulation outside surface – Case 1

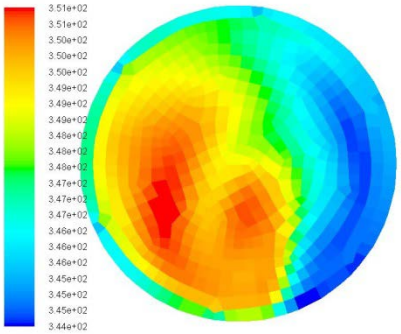

Figure 10 Temperature contours [K] on outlet face – Case 1

Table 4 Summary 3-D Conjugate heat transfer results (Cases 1 and 2)

Case	Outlet temperature (experimental/theoretical)	Outlet temperature (CFD)	Heat lost through cavity aperture
		[K]	[W]
1a	322	347.8	200.7
1b	322	318.3	79.40
2	1143	1100	6340

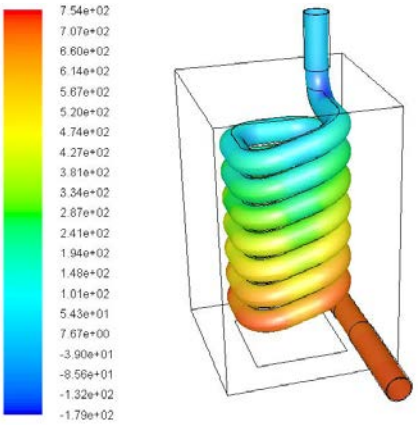

Figure 11 Static pressure contours [Pa] on tube walls – Case 1

CONCLUSIONS

The paper provided a CFD analysis of a parabolic dish tubular cavity receiver. The two-stage CFD approach solving first for the RTE and then performing a conjugate heat transfer simulation was found to be an effective method. Computational cost was lowered by considering an axi-symmetric model alongside a coarser 3-D model of the optical solution. Two conditions were evaluated and future work will consider reasons for deviations from experimental and theoretical results.

ACKNOWLEDGEMENTS

The authors would like to acknowledge the support from the University of Pretoria (South Africa) and the South African National Research Foundation (DST-NRF Solar Spoke).

REFERENCES

[1] Siva Reddy, V., Kaushik, S.C., Ranjan, K.R., Tyagi, S.K., State-of-the-art of solar thermal power plants – A review, *Renewable and Sustainable Energy Reviews*, 2013, Vol.27, pp. 258-273.

[2] Mancini, T., Heller, P., Butler, B. Osborn, B., Schiel, W., Goldberg, V., Buck, R., Diver, R., Andraka, C., Moreno, J., Dish-stirling systems: An overview of development and status, Journal of Solar Energy Engineering, 2003, Vol. 125, pp. 135-151.

[3] Le Roux, W.G., Bello-Ochende, T. and Meyer, J.P., The efficiency of an open-cavity tubular solar receiver for a small-scale solar thermal Brayton cycle, *Energy Conversion and Management*, 2014, Vol.84, pp. 457-470.

[4] Le Roux, W.G., Bello-Ochende, T. and Meyer, J.P.., Experimental testing of a tubular cavity receiver for a small-scale solar thermal Brayton cycle, *SASEC2015*, Kruger National Park, South Africa.

[5] Ávila-Marín, A.L., 2011. Volumetric receivers in Solar Thermal Power Plants with Central Receiver System technology: A review. Solar Energy, 85:891–910.

[6] M.F. Modest, Radiative Heat Transfer, Elsevier, 3rd edition, 2013.

[7] ANSYS Fluent Theory Guide, ANSYS v.14.5, 2013.

[8] Chai, J.C. and Patankar, S.V., Discrete-ordinates and finite-volume methods for radiative heat transfer, chapter in Handbook of Numerical Heat Transfer, 2nd Ed., John Wiley & Sons, 2006.

[9] Craig, K.J., Harkness, A.W., Kritzinger, H.P. & Hoffmann, J.E., Analysis of AP1000 reactor vessel cavity and support cooling, Paper ECN2010-A0459, European Nuclear Conference (ENC2010), 30 May - 2 June 2010, Barcelona, Spain.